Internal Report No. 88

Heavy Ion Calibration of Siemen's 5mm x 35cm^2 Detector

by

Alan C. Cummings
Richard A. Mewaldt
Brian Newport

Space Radiation Laboratory
California Institute of Technology
Pasadena, California
24 January 1983

1. Introduction

The Siemen's 5mm x 35cm^2 detector was exposed to heavy ions ($1 \leq Z \leq 18$, $0 \leq E/n \leq 720$ MeV/nuc) at the Bevalac in Berkeley during April 1981. This detector was one of several detectors of various thicknesses and areas that were being calibrated at the same time; however, it is the only 5mm-thick detector we have ever calibrated.

The overall goal of the calibration of the Siemen's detector was to determine whether or not the device is suitable as a particle-sensing element of a heavy-ion cosmic-ray isotope telescope. The relative scarcity of the heavy ions ($3 \leq Z \leq 28$) in the cosmic rays demands a detector of large area, and in order to have a large energy range it is also convenient to have thick detectors to minimize the number of separate elements that are normally stacked together in such telescopes. The 5mm x 35cm^2 Siemen's device is the largest-volume lithium-drifted detector that we know of and therefore an attractive possibility for our cosmic ray telescopes.

The important parameters of detectors we use are uniformity of thickness and charge collection, minimum deadlayer thickness, and, in the case of lithium-drifted detectors, an integral guard-ring which functions independently from the center active area. Our calibrations were designed to obtain data on each of these parameters. In addition, we hoped to demonstrate directly the isotope-resolving capability of a detector system which uses the 5mm detector by fragmenting the primary beam into particles of various charge, mass, and energy. In the following sections we briefly describe the experimental setup and then describe the results of the calibration.

2. Experimental Setup

A schematic representation of the experimental arrangement in the beam cave is shown in Fig. 1. There were 2 separate runs in which the Siemen's 5mm detector (hereafter labeled 5-1) was used. In the thickness-mapping run (detector stack 8) it was the middle detector in a stack of 5 detectors. In the fragmentation run (using stack 14) it was the 7th detector in a stack of 9 detectors and was sandwiched between 3mm-thick detectors of comparable area (3-3 in front and 3-4 behind). The detectors were mounted at an angle of 5° with respect to the beam because previous measurements by us and other groups have shown that the resolution of LiD devices for heavy ions is sometimes degraded for nuclei incident at 0° (normal incidence). The beam spot size was adjusted so that we had nearly uniform coverage of the entire area of our detectors. Pulseheights from all the detectors were recorded for each event which triggered the multiwire proportional counters.

3. Center/Guard Performance

One of the features of a double-grooved lithium-drifted detector such as the Siemen's device is that an anti-coincidence shield is incorporated directly into the detector. This annular shield surrounding the center active area is separated from it by a narrow groove (~1 mm wide). It is important that the two regions act essentially independent of each other.

In Fig. 2 we show the first of three plots which demonstrate this independence. The plot was made from the x-y positions recorded in the multiwire proportional counter (MWPC) for those particles which triggered the guard region but not the center active area of the detector. As expected, a well-defined annular ring is observed corresponding to the size and shape of the guard ring. In Fig. 3 the x-y positions of particles which triggered the center but not the guard are shown. Again the result is a "particle-picture" of the center region. (The vertical and horizontal banding in this figure is an artifact of the plotter and not a real feature of the data). Note that particles which fall in unexpected areas of Figs. 2 and 3 are due to a number of effects which produce erroneous position: two particles at the same time, particles which fragment, particles which produce knock-on electrons in the proportional counters, etc. This general background is typically very small (e.g., in Fig. 2 probably < 1%) and does not represent a problem with the detector.

Figure 4 shows a histogram of pulseheights from particles triggering the center, but not the guard region. A dump of the histogram is also included. The prominent peak extending off scale is due to ~700 MeV/nuc ^{40}Ar; the smaller peaks are due to lower-Z fragments, created by ^{40}Ar fragmentation upstream and within the detector stack. Below Z ≃ 10 the peaks wash out because there may be two high-charged fragments at the same time. This plot also contains events fragmenting within the device itself, which gives a smear above and below the ^{40}Ar peak.

The charge division for particles which trigger both center and guard regions is illustrated in Fig. 5. The clustering of particles near the center of the plot represents events with two particles passing through the detector at the same time. The overall shape of the charge division curve is reasonable, e.g., the heavy concentration of events near pulseheights of 1200 represent those particles striking the center of the groove. We do not have an obvious interpretation for some of the more subtle features of Fig. 5, such as the banding near guard pulseheight 3000 (which may be due to the 5° orientation).

In general, the center/guard performance is as expected and the detector successfully incorporates an essentially independent anti-coincidence shield.

4. Thickness Uniformity

It is not possible for us to separate the effects of a non-uniform charge collection response from thickness variations of the active area. Therefore, we are lumping the effects together and labeling all such variations as thickness variations. Furthermore, in the analysis done so far we have derived only a radial thickness profile from the data. Based on prior experience with 3mm-thick detectors in which azimuthal variations have typically been smaller than the radial ones, we have divided the detector into concentric annular regions and determined the mean thickness in each region. Because an absolute energy calibration was not done for this detector/electronics combination, our absolute thickness measurements are only good to ~10%. However, the relative thickness from one region to another is much more accurate.

Figure 6 shows an example histogram of the pulseheights obtained from a monoenergetic beam of ^{40}Ar (E ~700 MeV/nuc) in the radial range 1 to 1.5 cm. The resolution (FWHM) is ~2.8%. The data in each radial range and in the entire center active area of the detector is given in Table 1. For these runs the guard region of the detector was ignored.

In Fig. 7 we show the calculated radial thickness variation as measured in all 5 concentric annular regions out to a radius of 3 cm. The thickness of the detector appears to decrease at larger radial positions. One process that contributes to the measured radial thickness profile is that some energy is not collected due to knock-ons escaping the detector. This effect is difficult to estimate quantitatively but such escape is easier near the edge of the detector than near the center.

The radial thickness gradient shown in Fig. 7 has an adverse affect on the mass resolution of a telescope system employing the detector as a ΔE device if such variations are not taken into account using a thickness map. The mass resolution due to thickness variations is given approximately by

$$\frac{\sigma_m}{m} \approx 1.3 \frac{\sigma_l}{l}$$

where σ_m is the standard deviation in the mass, m, and σ_l is the standard deviation in the thickness, l, of the detector measured over the spatial resolution of the telescope. Typically the position-sensing elements of the most advanced cosmic ray telescopes give a position resolution of ~1 mm. For the line shown connecting the three middle points of Fig. 7 the gradient is ~0.034 %/mm. The corresponding σ_l / l is given approximately by :

$$\frac{\sigma_l}{l} \approx \frac{.034}{4} = .009\%$$

For Fe nuclei with mass 56 (typically the highest mass detected by such

systems),

$$\sigma_m \approx (56)(1.3)(.00009) = .007 \text{ amu.}$$

Typically, Landau fluctuations in the energy loss and other effects limit the overall resolution to ~0.25 amu for Fe. Therefore the contribution to the mass resolution due to the radial gradient shown in Fig. 7 is negligible.

The data taken during this run would enable a relative thickness map to be constructed on a scale of ~1 mm^2. No complete thickness maps for any of the detectors in the calibration have yet been made. However, some information on possible azimuthal gradients can be inferred from Table 1. If Landau fluctuations in the energy loss dominate the thickness variations (and/or charge collection non-uniformities) then the ratio σ/peak in Table 1 should be independent of position. However, the data for 5-1 show an increase in this parameter with radius indicating that azimuthal thickness variations or charge collection non-uniformities might be making a non-negligible contribution. If we assume for the moment that azimuthal thickness variations are responsible and further that these variations are negligible in the center 1-cm-radius data, then

$$\left[\frac{\sigma_l}{l}\right]_{\Delta Z} \approx \frac{\sqrt{49.7^2 - 43.8^2}}{3760} = .0062$$

$$\rightarrow \sigma_m = 0.45 \text{ for } {}^{56}\text{Fe}$$

$$= 0.33 \text{ for } {}^{40}\text{Ar}$$

Thus it would be necessary to correct for such azimuthal variations in order to achieve the required mass resolution.

5. Fragmentation Runs

The fragmentation runs provide a direct demonstration of the isotope-resolving capabilities of a detector system. In Fig. 8 the energy lost in a front detector (3-3) is plotted versus the energy lost in the following detector (5-1) for those particles which stop in the second detector. The heavy band is due to the primary beam, ^{40}Ar. The beam has passed through a variable-thickness target so particles of various energies are produced. Several other major bands appear due to other elements produced in the fragmentation process. Within each major band are smaller scale stripes due to different isotopes. The isotopic resolution displayed here for particles incident at 5° is excellent.

In Fig. 9 we show a similar plot, but in this case the first detector is the 5mm device and the following detector is 3mm thick. The striping due to

isotopes is not nearly as obvious as in Fig. 8. The resolution is not as good and the isotope tracks have blended together. Because we have illuminated the entire detector and have not corrected for thickness variations it is not possible to tell at this time to what extent the resolution could be improved if, for example, the radial and/or azimuthal variations were taken into account.

Among the possible explanations for the differences in Fig. 8 and 9 are:

1) Azimuthal thickness variations or charge collection non-uniformities may be worse in the 5mm detector than they are in the 3mm one. Indeed the magnitude of the mass resolution contribution to possible azimuthal thickness variations was estimated in Section 4 for the 5mm detector to be ~0.33 amu for ^{40}Ar which is probably enough to account for the lack of good isotope separation. (The contribution to the mass resolution due to the radial variation shown in Fig. 7 is somewhat smaller, $\leq$ 0.10 amu for ^{40}Ar, and probably not enough by itself to account for the poor resolution observed.)

2) Variations in the thicker deadlayer of the 5mm device may be significant. In Fig. 8 the size of the deadlayer can be estimated from the "foldback" of the tracks near the maximum energy loss in 5-1. This foldback is due primarily to the deadlayer in 5-1. (The detector was oriented such that the deadlayer was at the beam-exit side of the detector. Approximately 9 μ of silicon equivalent air gap and ~6 μ of range in the following detector are also included in this foldback.) From the foldback in Fig. 8 we have estimated the deadlayer to be ~165 μ ($\pm$10 μ). In contrast, the deadlayer on the 3mm detector (3.3) is ~15 μ (from laboratory measurements using ~6 MeV α particles). It is possible that variations in the thicker deadlayer of the 5mm detector cause part of the loss of resolution observed in the isotope track plot of Fig. 9. It would be desirable to have thinner deadlayers but it may also be possible to map both the active thickness and the deadlayers well enough to correct for such effects.

6. Conclusions

With regard to the 5mm detector's use as a ΔE device in a cosmic ray telescope with 1mm position information:

1) The center/guard performance is acceptable.

2) The radial thickness variations, while not negligible, are acceptable.

3) The isotopic-resolving capability may be acceptable but it was not directly demonstrated. Thinner deadlayers would be a definite improvement. Azimuthal thickness variations were not measured directly but could be responsible for degradation in the resolution. Thickness maps to 0.1%

accuracy will be required before a final determination of the detector's usefulness in such telescopes is made.

Table 1. Thickness Uniformity of Detector 5-1

r_1 (cm)	r_2 (cm)	Peak (Channels)	sigma (Channels)	sigma/Peak %	$sigma_{mean}$ (Channels)	Relative Thickness %
0.0	1.0	3781.1	43.8	1.16	0.3	100.00 +- .06
1.0	1.5	3775.4	44.4	1.18	0.3	99.83 +- .09
1.5	2.0	3769.6	47.1	1.25	0.2	99.68 +- .09
2.0	2.5	3762.6	47.4	1.26	0.2	99.49 +- .09
2.5	3.0	3748.5	52.8	1.41	0.3	99.13 +- .09
all of center		3760.0	49.7	1.32	-	-

FIGURE CAPTIONS

Figure 1. Experimental setup in beam cave area as viewed from ceiling.

Figure 2. X versus Y positions in the MWPC for particles triggering only the guard ring of detector 5-1. The scale has ~ 70 units/mm.

Figure 3. X versus Y positions in the MWPC for particles triggering only the center active area of detector 5-1.

Figure 4. Pulseheight histogram for particles triggering the center active area of detector 5-1. The peak near channel 3750 is due to the primary beam of ~700 MeV/nuc ^{40}Ar. The smaller peaks at lower channel numbers correspond to lower-Z fragments of the primary beam.

Figure 5. Pulseheight in center versus pulseheight in guard for those particles triggering both.

Figure 6. Pulseheight histogram for monoenergetic beam of ~700 MeV/nuc ^{40}Ar. The data is from the radial range 1 to 1.5 cm.

Figure 7. Calculated thickness relative to center versus radius.

Figure 8. Energy lost in front detector 3-3 versus that lost in stopping detector 5-1. The major bands are due to elements produced by fragmentation in the target. The fine scale striping within the major bands is due to isotopes of the elements.

Figure 9. Energy lost in front detector 5-1 versus that lost in stopping detector 3-4. The major bands are due to elements produced by the fragmentation target. The fine scale striping within the major bands that was obvious in Fig. 8 is not so clear here.

Experimental Setup in Beam Cave
(looking down from ceiling)

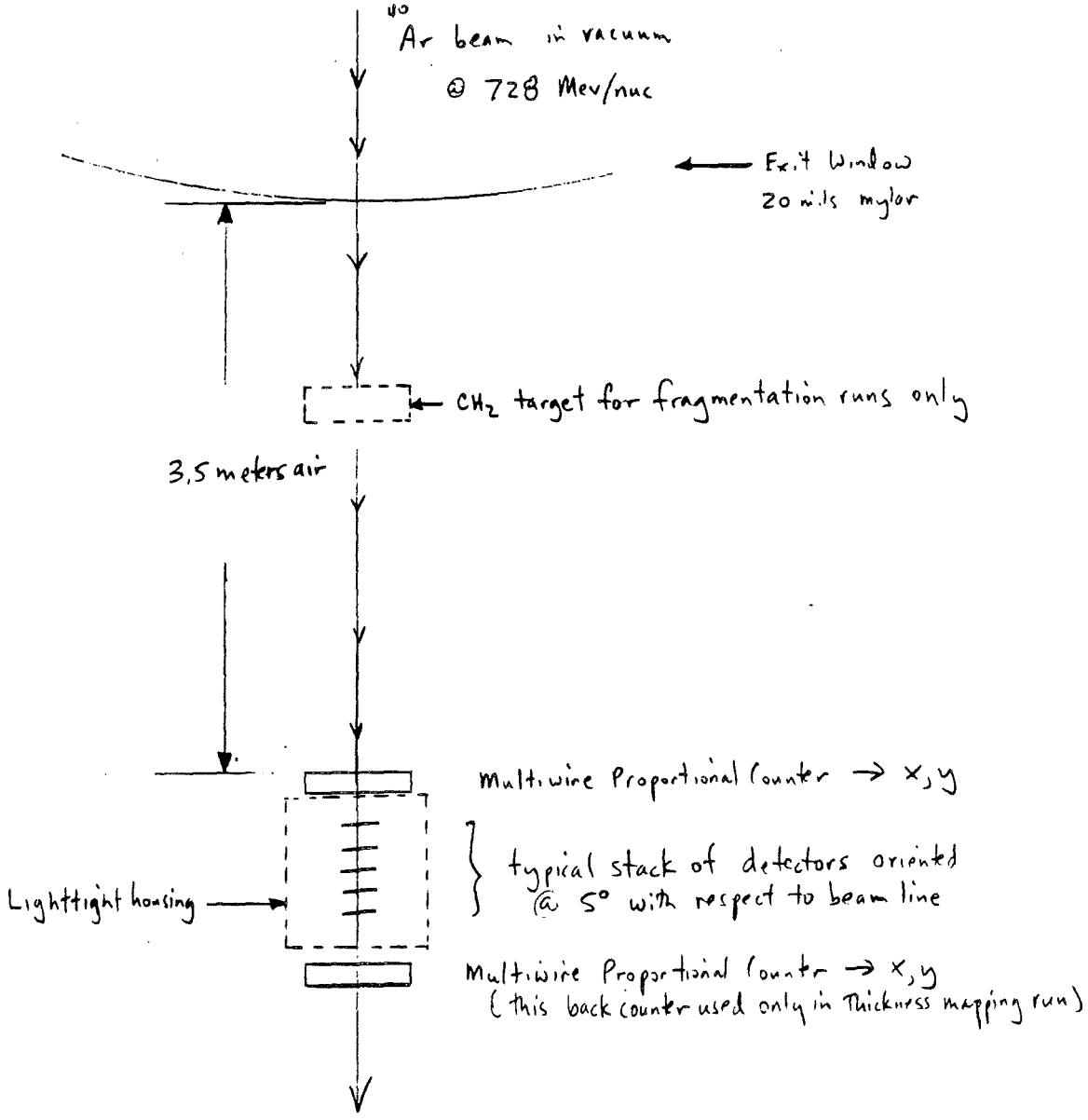

Figure 1 (not to scale)

tag masks: ignr = 37400 true = 100377 total points plotted: 15336

exttag masks: ignored total points rejected: 484664

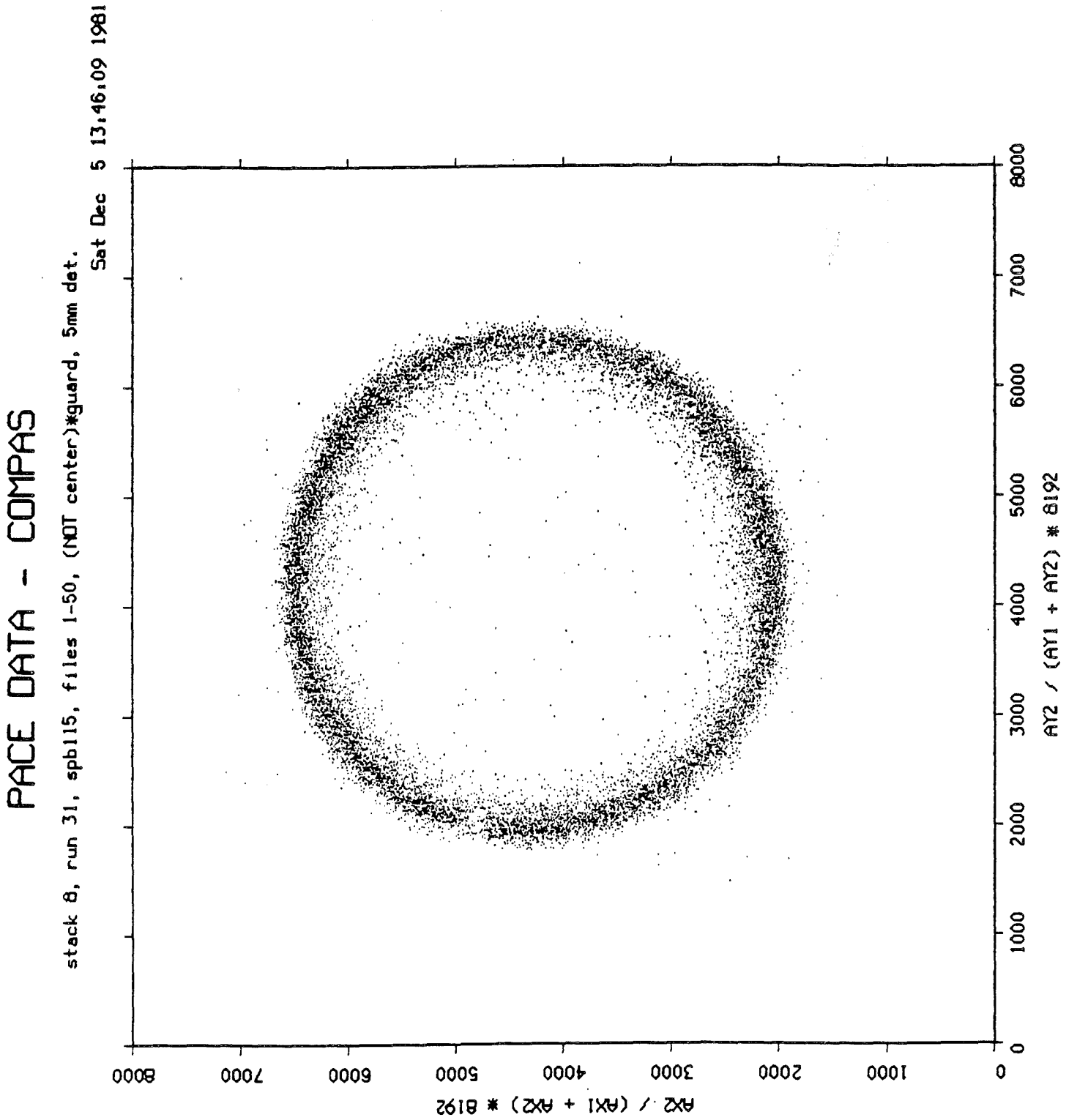

Fig. 2

tag masks: ignr = 37400 true = 40377 total points plotted: 193775

exttag masks: ignored total points rejected: 306225

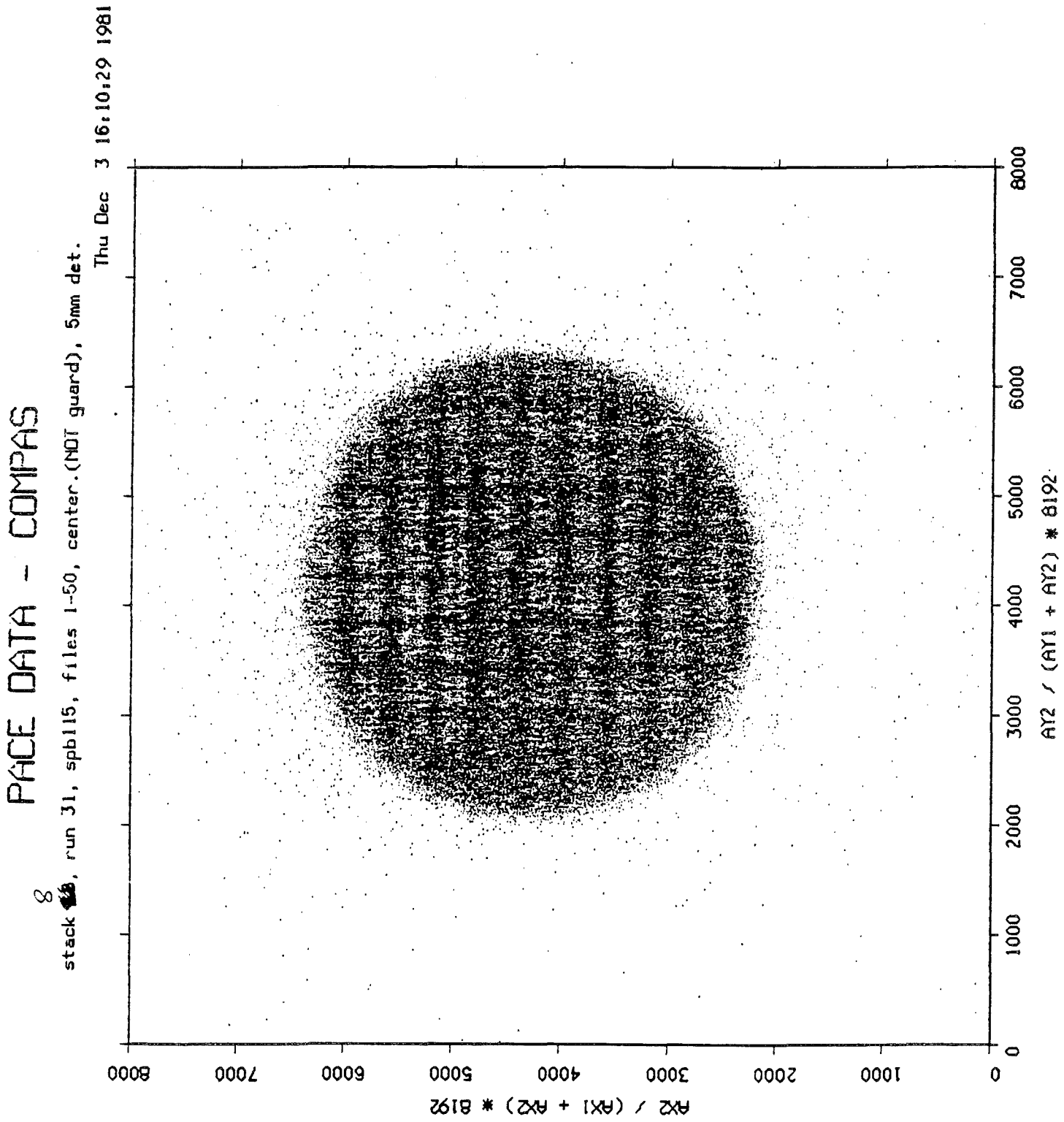

Fig. 3

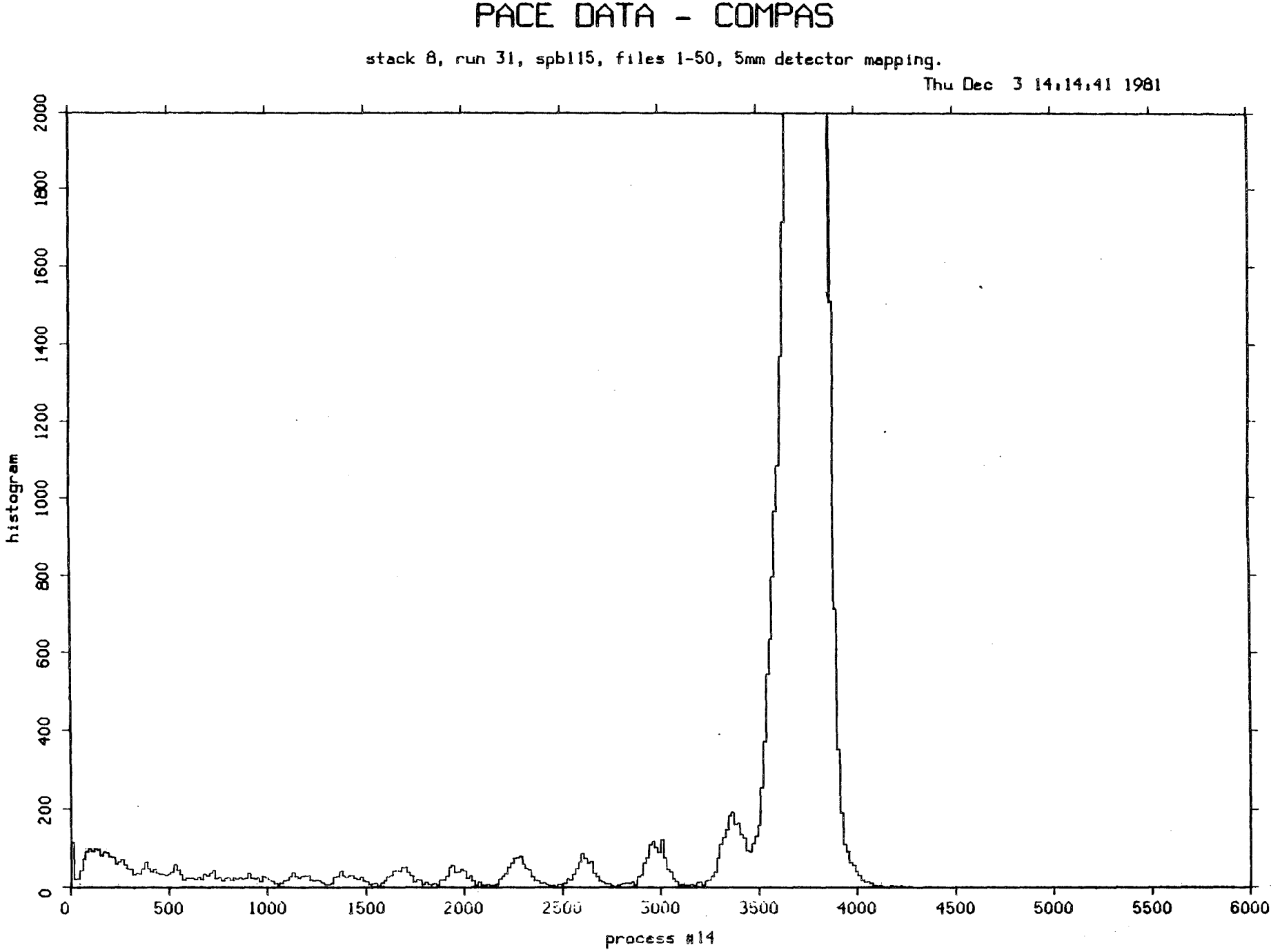
PACE DATA - COMPAS
stack 8, run 31, spb115, files 1-50, 5mm detector mapping.
Thu Dec 3 14:14:41 1981
histogram
process #14
0
200
400
600
800
1000
1200
1400
1600
1800
2000
0
500
1000
1500
2000
2500
3000
3500
4000
4500
5000
5500
6000

Fig. 4

0:	118	15:	19	30:	20	45:	42	60:	71
75:	90	90:	98	105:	92	120:	97	135:	94
150:	82	165:	89	180:	88	195:	78	210:	77
225:	59	240:	65	255:	71	270:	57	285:	47
300:	46	315:	32	330:	37	345:	35	360:	48
375:	65	390:	48	405:	40	420:	46	435:	36
450:	33	465:	33	480:	30	495:	35	510:	40
525:	58	540:	44	555:	32	570:	18	585:	22
600:	22	615:	22	630:	19	645:	25	660:	19
675:	33	690:	29	705:	37	720:	43	735:	20
750:	24	765:	16	780:	22	795:	23	810:	18
825:	23	840:	21	855:	23	870:	21	885:	22
900:	37	915:	22	930:	21	945:	23	960:	14
975:	27	990:	24	1005:	19	1020:	16	1035:	10
1050:	7	1065:	9	1080:	16	1095:	17	1110:	26
1125:	38	1140:	26	1155:	22	1170:	27	1185:	29
1200:	29	1215:	18	1230:	16	1245:	18	1260:	15
1275:	11	1290:	7	1305:	6	1320:	10	1335:	25
1350:	27	1365:	41	1380:	29	1395:	23	1410:	28
1425:	28	1440:	22	1455:	19	1470:	25	1485:	15
1500:	14	1515:	6	1530:	8	1545:	9	1560:	2
1575:	9	1590:	16	1605:	25	1620:	28	1635:	41
1650:	45	1665:	41	1680:	50	1695:	50	1710:	38
1725:	28	1740:	12	1755:	19	1770:	17	1785:	7
1800:	12	1815:	6	1830:	7	1845:	10	1860:	5
1875:	18	1890:	18	1905:	26	1920:	50	1935:	55
1950:	38	1965:	40	1980:	45	1995:	43	2010:	22
2025:	28	2040:	15	2055:	5	2070:	13	2085:	5
2100:	5	2115:	6	2130:	3	2145:	4	2160:	7
2175:	20	2190:	27	2205:	35	2220:	50	2235:	62
2250:	74	2265:	76	2280:	78	2295:	60	2310:	49
2325:	46	2340:	26	2355:	18	2370:	16	2385:	9
2400:	11	2415:	7	2430:	5	2445:	5	2460:	2
2475:	6	2490:	7	2505:	10	2520:	21	2535:	17
2550:	31	2565:	47	2580:	65	2595:	86	2610:	74
2625:	61	2640:	66	2655:	36	2670:	27	2685:	15
2700:	12	2715:	8	2730:	8	2745:	4	2760:	1
2775:	4	2790:	6	2805:	9	2820:	11	2835:	9
2850:	12	2865:	5	2880:	25	2895:	30	2910:	61
2925:	75	2940:	109	2955:	116	2970:	103	2985:	89
3000:	121	3015:	75	3030:	45	3045:	39	3060:	20
3075:	14	3090:	5	3105:	6	3120:	4	3135:	4
3150:	6	3165:	4	3180:	11	3195:	12	3210:	5
3225:	16	3240:	17	3255:	26	3270:	40	3285:	75
3300:	111	3315:	128	3330:	148	3345:	182	3360:	191
3375:	160	3390:	163	3405:	135	3420:	126	3435:	95
3450:	91	3465:	112	3480:	131	3495:	159	3510:	254
3525:	370	3540:	543	3555:	633	3570:	796	3585:	963
3600:	1081	3615:	1368	3630:	1714	3645:	2519	3660:	3733
3675:	5310	3690:	8407	3705:	11730	3720:	16159	3735:	19783
3750:	21567	3765:	22122	3780:	20652	3795:	18258	3810:	13218
3825:	9043	3840:	5708	3855:	3130	3870:	1510	3885:	712
3900:	351	3915:	190	3930:	111	3945:	92	3960:	63
3975:	57	3990:	41	4005:	28	4020:	17	4035:	13
4050:	14	4065:	9	4080:	3	4095:	3	4110:	3

Dump of Fig. 4

4125:	1	4140:	1	4155:	2	4170:	3	4185:	1
4200:	0	4215:	3	4230:	2	4245:	1	4260:	1
4275:	0	4290:	0	4305:	0	4320:	0	4335:	0
4350:	0	4365:	0	4380:	0	4395:	0	4410:	0
4425:	0	4440:	0	4455:	0	4470:	0	4485:	0
4500:	0	4515:	0	4530:	0	4545:	0	4560:	0
4575:	0	4590:	0	4605:	0	4620:	0	4635:	0
4650:	0	4665:	0	4680:	0	4695:	0	4710:	0
4725:	0	4740:	0	4755:	0	4770:	0	4785:	0
4800:	0	4815:	0	4830:	0	4845:	0	4860:	0
4875:	0	4890:	0	4905:	0	4920:	0	4935:	0
4950:	0	4965:	0	4980:	0	4995:	0	5010:	0
5025:	0	5040:	0	5055:	0	5070:	0	5085:	0
5100:	0	5115:	0	5130:	0	5145:	0	5160:	0
5175:	0	5190:	0	5205:	0	5220:	0	5235:	0
5250:	0	5265:	0	5280:	0	5295:	0	5310:	0
5325:	0	5340:	0	5355:	0	5370:	0	5385:	0
5400:	0	5415:	0	5430:	0	5445:	0	5460:	0
5475:	0	5490:	0	5505:	0	5520:	0	5535:	0
5550:	0	5565:	0	5580:	0	5595:	0	5610:	0
5625:	0	5640:	0	5655:	0	5670:	0	5685:	0
5700:	0	5715:	0	5730:	0	5745:	0	5760:	0
5775:	0	5790:	0	5805:	0	5820:	0	5835:	0
5850:	0	5865:	0	5880:	0	5895:	0	5910:	0
5925:	0	5940:	0	5955:	0	5970:	0	5985:	0

tag masks: ignr = 25400 true = 152377 total points plotted: 21581

exttag masks: ignored total points rejected: 478419

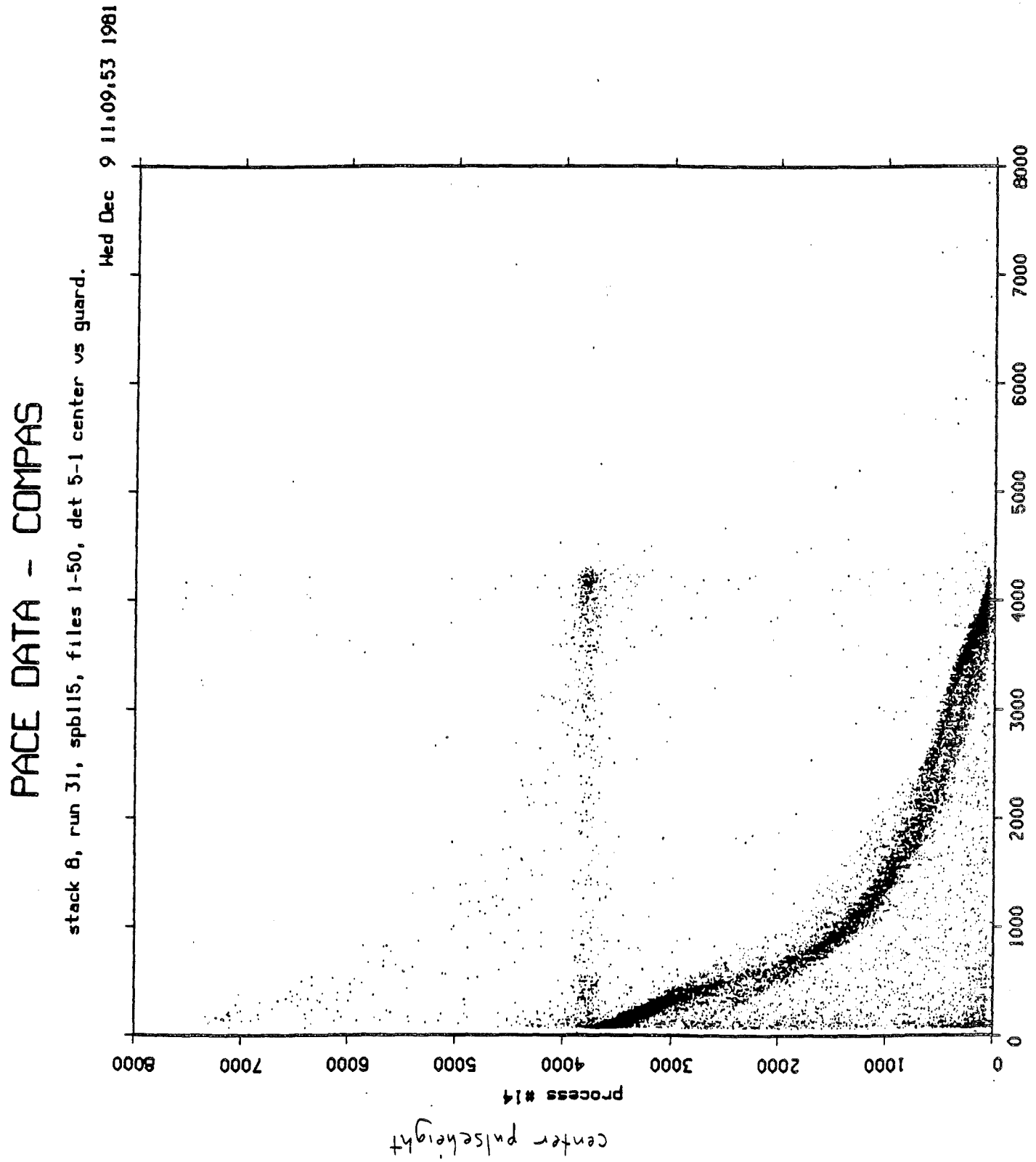

Fig. 5

PACE DATA - COMPAS

stack 8, run 31, spb115, files 1-50, 5mm det, 1 < radius < 1.5cm.

Sat Dec 5 15:06:20 1981

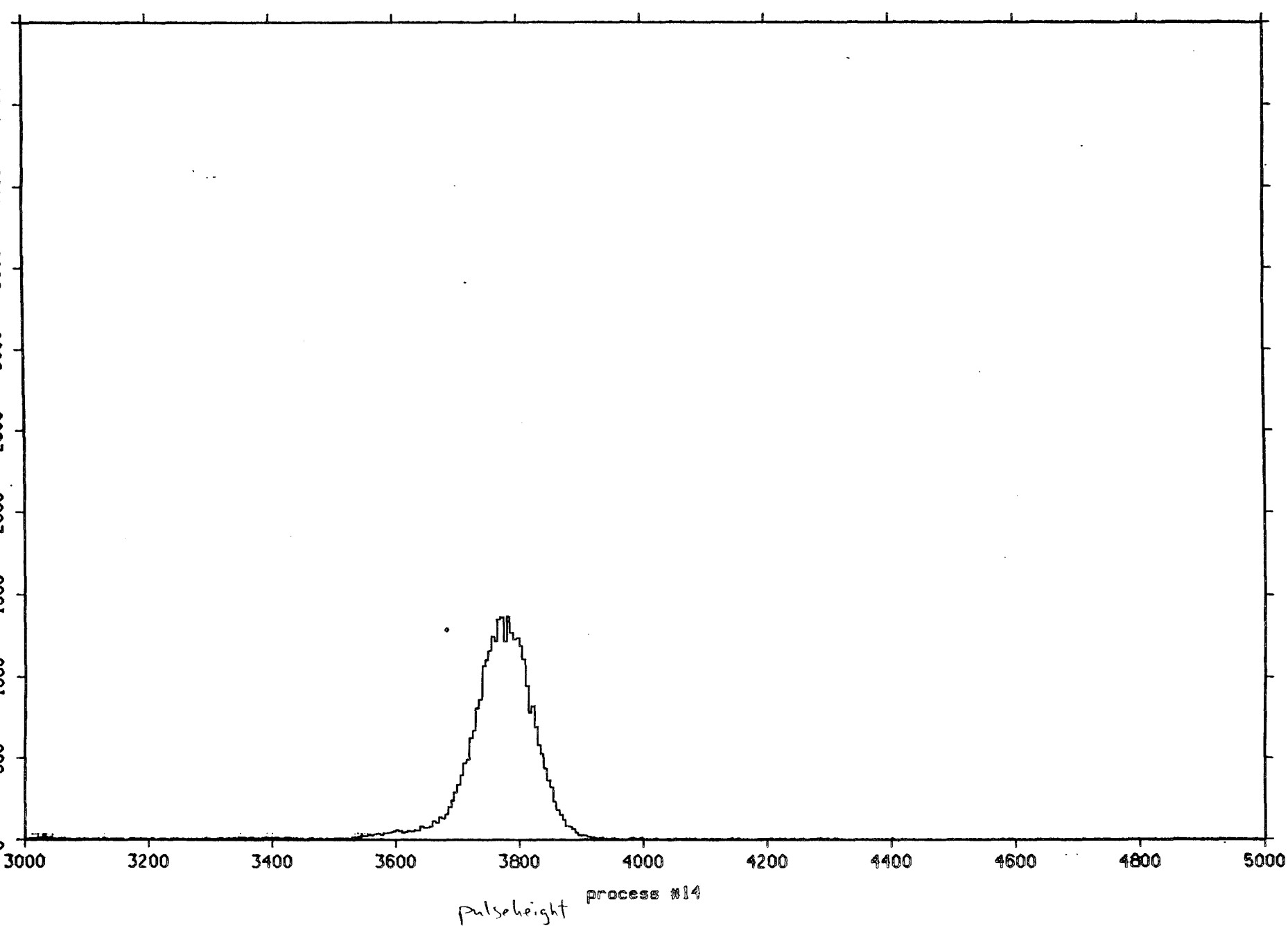

Fig 9

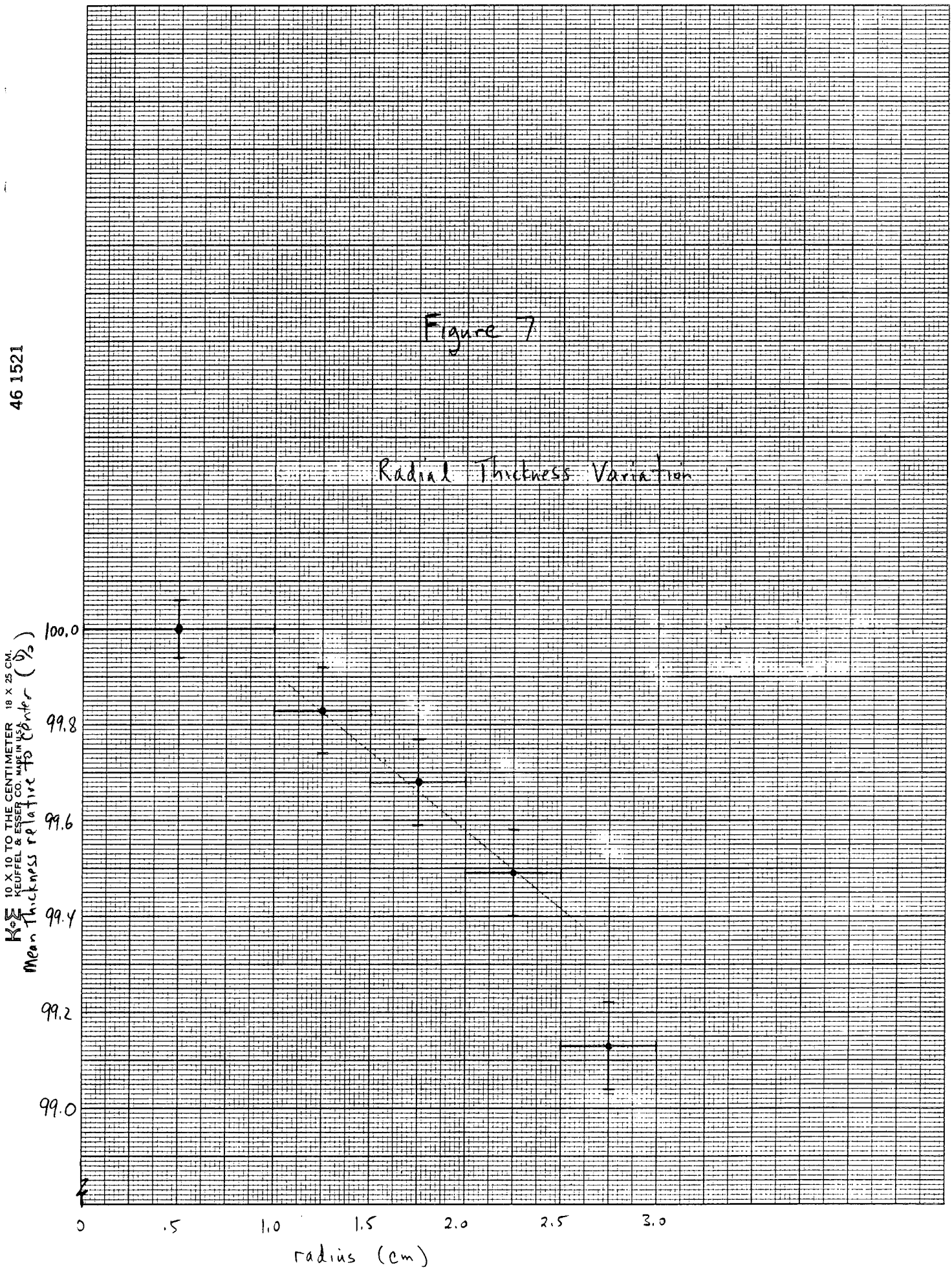

Figure 7

Radial Thickness Variation

1

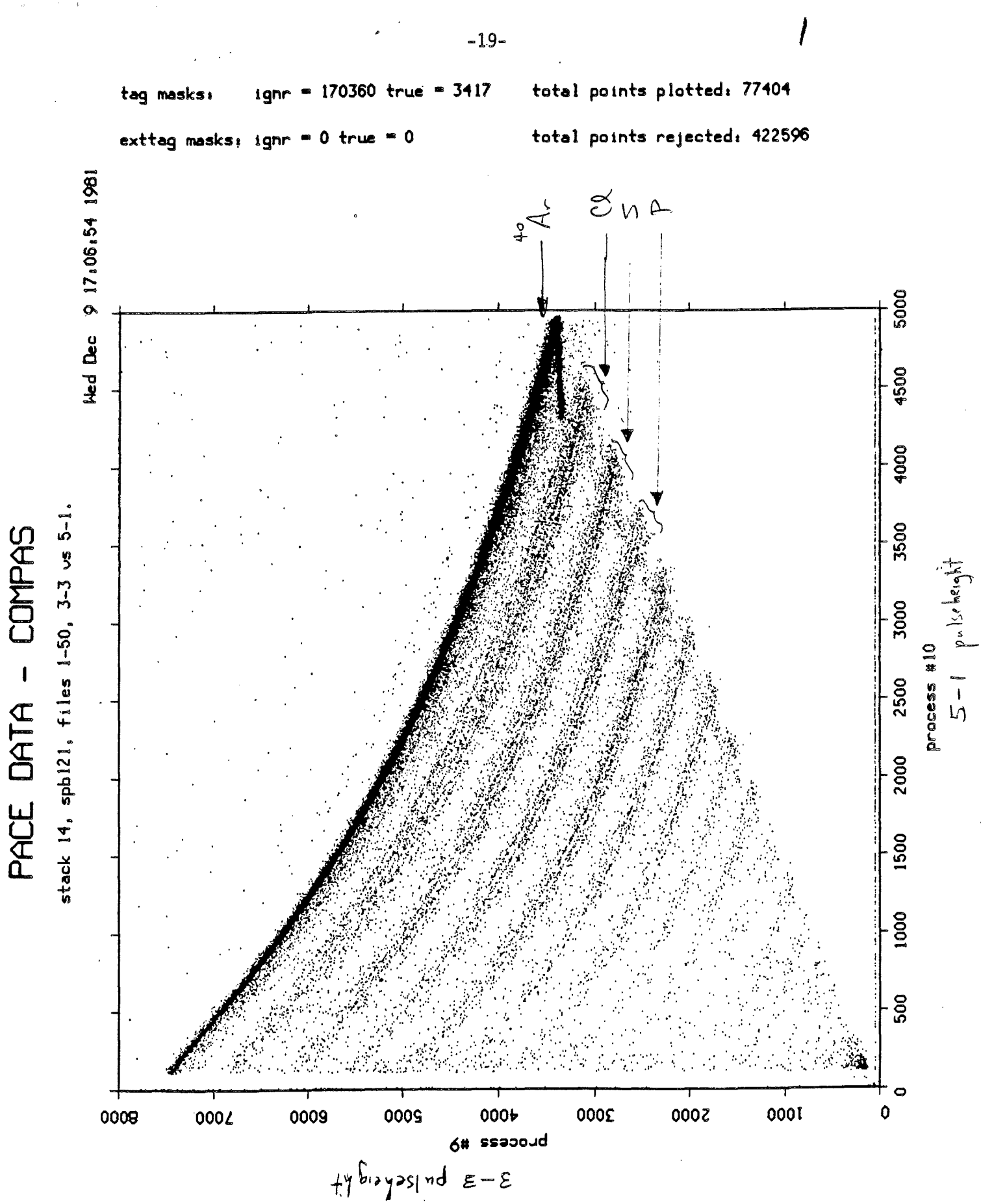
tag masks: ignr = 170360 true = 3417
total points plotted: 77404
exttag masks: ignr = 0 true = 0
total points rejected: 422596
Wed Dec 9 17:06:54 1981
PACE DATA - COMPAS
stack 14, spb121, files 1-50, 3-3 vs 5-1.
40Ar
α
S
P
process #9
process #10
5-1 pulseheight
3-3 pulseheight
0
500
1000
1500
2000
2500
3000
3500
4000
4500
5000
1000
2000
3000
4000
5000
6000
7000
8000

Fig. 8

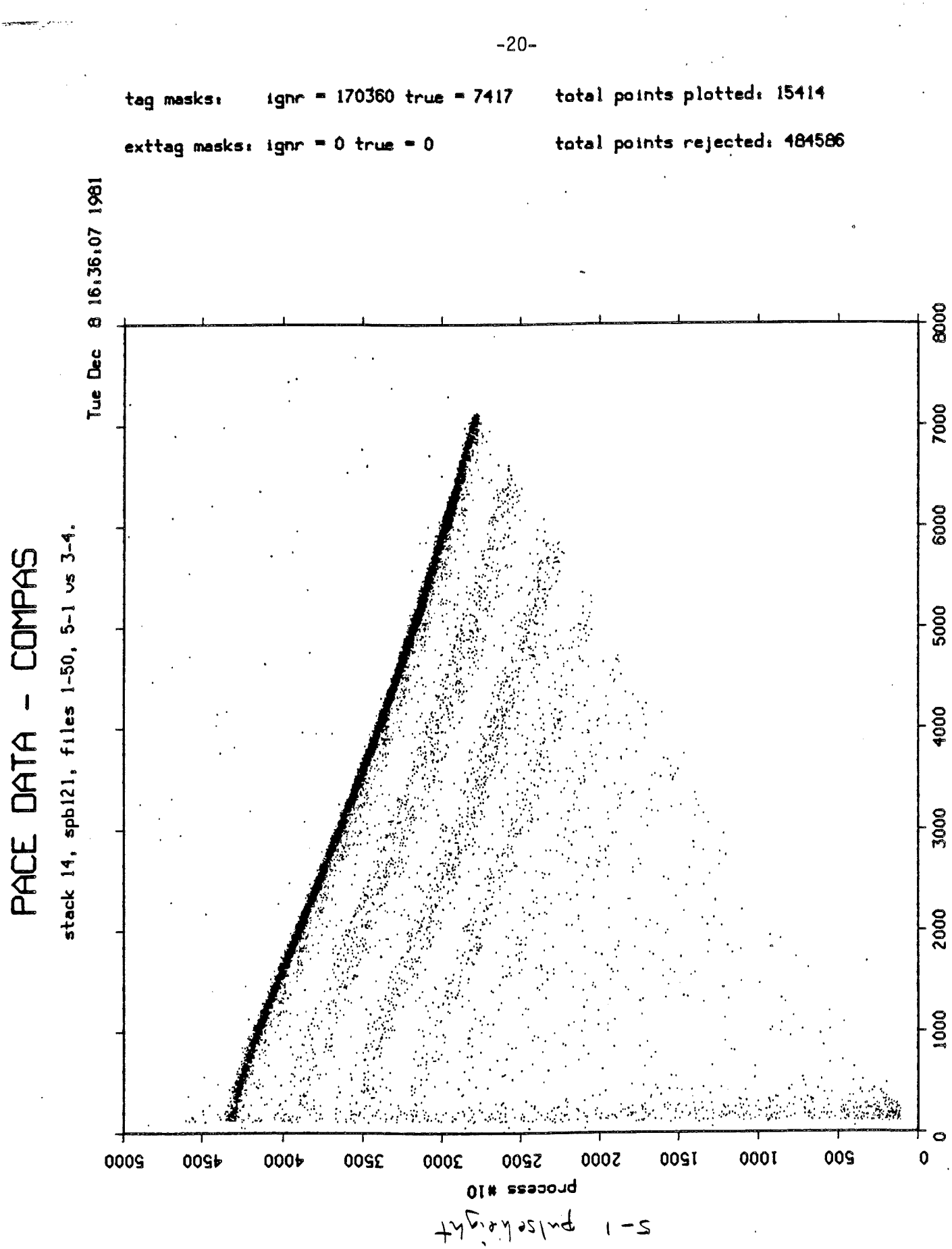
tag masks: ignr = 170360 true = 7417
total points plotted: 15414
exttag masks: ignr = 0 true = 0
total points rejected: 484586
PACE DATA - COMPAS
stack 14, spb121, files 1-50, 5-1 vs 3-4.
Tue Dec 8 16:36:07 1981
process #10
process #11
0
500
1000
1500
2000
2500
3000
3500
4000
4500
5000
1000
2000
3000
4000
5000
6000
7000
8000
5-1 pulseheight
3-4 pulseheight

Fig - 9